INSTITUTE OF PHYSICS PUBLISHING MODELLING AND SIMULATION IN MATERIALS SCIENCE AND ENGINEERING

Modelling Simul. Mater. Sci. Eng. **14** (2006) 799–816 doi:10.1088/0965-0393/14/5/001

Cracking and adhesion at small scales: atomistic and continuum studies of flaw tolerant nanostructures

Markus J Buehler[1,4], Haimin Yao[2], Huajian Gao[2] and Baohua Ji[3]

[1] Department of Civil and Environmental Engineering, Massachusetts Institute of Technology, 77 Massachusetts Ave, Cambridge, MA, 02139, USA
[2] Max Planck Institute for Metals Research, Heisenbergstrasse 3, D-70569, Stuttgart, Germany
[3] Department of Engineering Mechanics, Tsinghua University, Beijing, People's Republic of China

E-mail: mbuehler@MIT.EDU

Received 21 October 2005, in final form 27 February 2006
Published 30 May 2006
Online at stacks.iop.org/MSMSE/14/799

Abstract

Once the characteristic size of materials reaches nanoscale, the mechanical properties may change drastically and classical mechanisms of materials failure may cease to hold. In this paper, we focus on joint atomistic-continuum studies of failure and deformation of nanoscale materials. In the first part of the paper, we discuss the size dependence of brittle fracture. We illustrate that if the characteristic dimension of a material is below a critical length scale that can be on the order of several nanometres, the classical Griffith theory of fracture no longer holds. An important consequence of this finding is that materials with nano-substructures may become flaw-tolerant, as the stress concentration at crack tips disappears and failure always occurs at the theoretical strength of materials, regardless of defects. Our atomistic simulations complement recent continuum analysis (Gao *et al* 2003 *Proc. Natl Acad. Sci. USA* **100** 5597–600) and reveal a smooth transition between Griffith modes of failure via crack propagation to uniform bond rupture at theoretical strength below a nanometre critical length. Our results may have consequences for understanding failure of many small-scale materials. In the second part of this paper, we focus on the size dependence of adhesion systems. We demonstrate that optimal adhesion can be achieved by either length scale reduction, or by optimization of the shape of the surface of the adhesion element. We find that whereas change in shape can lead to optimal adhesion strength, those systems are not robust against small deviations from the optimal shape. In contrast, reducing the dimensions of the adhesion system results in robust adhesion devices that fail at their theoretical strength, regardless of the presence of flaws. An important consequence of this finding is that even under the presence of surface roughness, optimal adhesion is possible provided the size of contact elements is sufficiently small. Our

[4] Author to whom any correspondence should be addressed.

atomistic results corroborate earlier theoretical modelling at the continuum scale (Gao and Yao 2004 *Proc. Natl Acad. Sci. USA* **101** 7851–6). We discuss the relevance of our studies with respect to nature's design of bone nanostructures and nanoscale adhesion elements in geckos.

(Some figures in this article are in colour only in the electronic version)

1. Introduction

With continued miniaturization of technologies, for example those achieved in N/MEMS technologies or in lab-on-a-chip devices, it is critical to understand the behaviour of materials at ultra-small length scales reaching down to several nanometres. In several previous studies, it has been suggested that once the characteristic size of materials reaches nanoscale, the mechanical properties may change drastically. For example, changes in materials behaviour as a function of dimension have been confirmed in numerous experimental, theoretical and computational studies of materials including nanocrystalline metals [1–7] and thin metal films [8–12]. Molecular dynamics (MD) modelling has been a fruitful approach that has helped to understand deformation mechanisms of nanocrystalline, primarily ductile materials [6, 7]. In recent continuum level studies, it has been shown that classical mechanisms of materials failure such as brittle fracture cease to hold [13–15] once the material reaches dimensions close to a few nanometres [13, 14, 16]. However, up to date, few atomistic studies have been carried out focusing on the fracture mechanics of brittle materials at extremely small scales. In this paper, we will use a combination of continuum theory and large-scale atomistic simulation to address the size dependence of brittle fracture and adhesion systems.

Small-scale materials with extremely tiny characteristic structures are often found in biological materials [17–22]. Nature is a master in building and using nano-devices to perform different tasks ranging from energy transport to assembling machines with complex control systems far beyond what human beings have ever been able to create. In particular, nature has achieved several classes of materials with superior properties, such as, for example, bone-like materials [13, 23] or adhesion systems [20, 21, 24]—all featuring the smallest structural details on the order of several to several hundred nanometres. It is a timely task to understand how nature designs these materials from a very fundamental, atomistic perspective, and to understand the impact of size reduction on the mechanics of materials.

In studies of microstructures of bone-like materials, it was discovered that biological bone-like materials consist of a generic microstructure characterized by staggered mineral platelets embedded in a soft matrix material consisting of collagen (see figure 1, left) [18]. Although the matrix material is as soft as human skin, and the mineral platelets are as brittle as classroom chalk, the combination of both materials in a nanostructure leads to superior mechanical properties. Is the nanometre length scale the secret for such superior properties? In other studies, it was established [16, 17, 19–21, 24] that nature can produce very strong adhesion systems based on relatively weak van der Waals interactions [24]. Using a contact area comparable with that of a human hand, geckos can stick strongly to a variety of chemically and mechanically different surfaces. In these systems, the size of the terminal adhesion elements is restricted to nanometre length scale [17, 19, 20]. For instance, in geckos, the spatula has a typical diameter on the order of 200 nm [16, 17]. Is restricting the length scale of the adhesion element to nanometre the key to providing such superior adhesion properties?

We hypothesize that in both bulk and surface materials, the design of the relevant structural links that sustain load transfer (e.g. the spatula in adhesion systems or the mineral platelets in

bone) is the key to understanding the properties of these materials. Scale reduction seems to be a common design principle found in biological materials to create structural links leading to robust designs.

We demonstrate that design at the nanometre scale may play a critical role in understanding the structure of many biological materials. Our central finding is that once characteristic materials length scales are reduced to nanoscale, mechanical properties may change dramatically and new phenomena may occur. For example, atomistic simulations reveal that stress concentrations at crack tips disappear in materials with sufficiently small dimensions.

This paper is divided into two main parts: In the first part, we discuss fracture in nanostructures, and in the second part we focus on ultra-small scale adhesion elements. In the first part of the paper, we consider a long crack embedded in a thin strip of material. We illustrate that if the width of the strip is much larger than the critical scale for flaw tolerant design, failure of the material is governed by the Griffith condition, in agreement with current understanding [25]. In contrast, if the width of the thin strip is below the critical size, the solid can sustain loads up to its theoretical strength, regardless of the existence of the crack. In the second part of the paper, large-scale atomistic studies of biological adhesion elements are used to demonstrate the influence of size reduction and surface morphology on the adhesion strength. We illustrate that reducing the size of contact elements leads to optimal adhesion and the stress concentration vanishes at pull-off. We conclude with a discussion of the results and the outlook of future investigations.

2. Strength of brittle nanoparticles

In this section, we focus on fracture properties of ultra small brittle particles and the impact of size variation on fracture properties.

The goal of these studies is to understand the limiting cases for the validity of Griffith's theory of fracture. In addition to general interest to understand if Griffith's theory can be applied to brittle fracture at ultra small scales, this study is motivated by the fact that in bone, mineral platelets appearing at ultra small nanoscale dimensions seem to play an integral role in the load transfer process. Thus, their properties may have implications on the strength of the bone. As illustrated in figure 1 (right), the mineral platelets are critical for the integrity of the material since they carry most of the tensile load. We thus focus on the fracture strength of the brittle platelets.

2.1. Theoretical considerations

We consider the strength of a small mineral particle with a crack under mode I tensile loading as shown schematically in figure 2. We assume that the classical continuum theory of fracture [26] can be applied to describe this material. From classical fracture mechanics, the critical stress for crack nucleation in this perfectly brittle material is given by the Griffith condition $G = 2\gamma$, where γ is the fracture surface energy and G is the energy release rate. For the strip geometry as shown in figure 2, with strip width ξ, the energy release rate can be expressed as

$$G = \frac{\sigma^2 \xi (1 - \nu^2)}{2E}, \tag{1}$$

where E is Young's modulus, ν is the Poisson ratio, and σ is the applied stress. At the critical point of onset of crack motion, the energy released per unit length of crack growth must equal the energy necessary to create a unit length of two new surfaces. Using the Griffith condition,

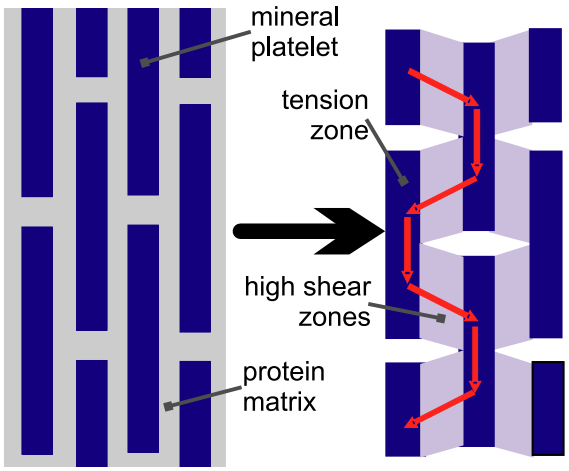

Figure 1. Bone-like materials consist of a hierarchical microstructure made of nanoscale constituents. Left: The plot depicts the microstructure of such bone-like biological materials at the smallest scale. Such materials typically consist of fragile, brittle mineral platelets embedded in protein matrix materials as soft as human skin. The combination of these two phases in a nanocomposite results in superior material properties. In our studies, we focus on the fracture properties of mineral platelets since they play a critical role in determining the strength of these materials. Right: The tension-shear chain model showing the path of load transfer in the mineral–protein composites. The mineral platelets carry a tensile load and the protein transfers loads between the platelets via shear. In this paper, we focus on the strength of the mineral platelets. (Figure adapted from [13].)

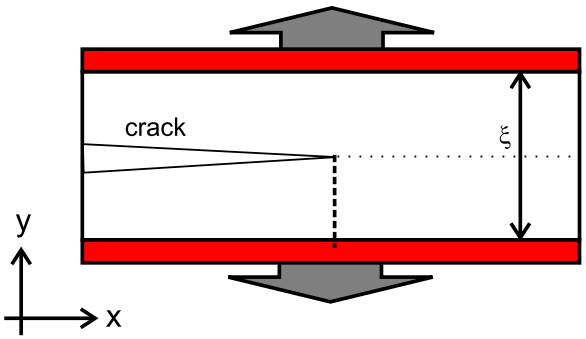

Figure 2. The geometry and dimensions of a cracked platelet. This model is used in our continuum and atomistic studies of fracture at small scales. We consider a thin strip of width ξ, in which the crack length extends half-way through the length of the slab in the x direction. The system is under mode I tensile loading as indicated in the plot (mode I loading in the y direction). This system resembles plane strain conditions.

equation (1) can be solved for the critical applied stress

$$\sigma = \sqrt{\frac{4\gamma E}{\xi(1-\nu^2)}} \tag{2}$$

for spontaneous onset of failure. For decreasing the layer width ξ equation (2) predicts an increasing stress for nucleation of the crack, approaching infinity as ξ goes to zero. This,

however, cannot be literally accepted, since the stress cannot exceed the theoretical strength of the material, which is denoted by σ_{th}. This immediately yields a critical layer width ξ_{cr} below which fracture cannot be described by the Griffith theory any more. Instead, the strength of the cracked slab is given by the theoretical strength of the material, regardless of the presence of a crack. This critical length can be calculated to be

$$\xi_{\text{cr}} = \frac{4\gamma E}{\sigma_{\text{th}}^2(1-\nu^2)}. \tag{3}$$

We note that similar expressions for critical length scales can be derived for a variety of geometries.

Further, the flaw-tolerance concept has recently also been discussed within the framework of Dugdale's model [27]. The analysis described in [27] has also shown the existence of the flaw-tolerance concept. In some sense, cohesive interactions between atoms, which are universal features of all materials, can be viewed as some sort of ultimate plastic deformation under extremely large stresses.

These considerations have led to the question whether the continuum theory based on the Griffith concept is still applicable at ultra-small nanoscales. Here we use atomistic simulation as a tool to gain further insight.

2.2. Atomistic modelling

Atomistic modelling of the strip crack problem is conducted by classical MD simulations using a modified IMD code [28] while utilizing a global energy minimization scheme. We use fully three-dimensional models to study crack nucleation and propagation.

Consider the geometry depicted in figure 2. The initial crack extends over half of the slab in the x direction. The slab size in the x direction is several times larger than that in the y direction. We assume an FCC crystal oriented in cubic orientations, with $x = [100]$, $y = [010]$ and $z = [001]$. The crystal is periodic in the z-direction with crack faces along the (010) planes.

We use the concept of virtual atom types to distinguish various atomic interactions and to allow application of boundary conditions. Atoms in the red region (figure 2) are assigned a specific virtual atom type and are displaced according to a prescribed displacement field.

We use an energy minimization scheme to relax the crystal after each increment of loading. An increment of strain of magnitude $\Delta\varepsilon_{yy} = 0.001$ is applied every $\Delta N = 3\,000$ integration steps. Different loading rates are chosen to ensure that the results have reached equilibrium before the next loading increment is applied. The loading is constant along the x-direction.

Interatomic potentials for a variety of different brittle materials exist, many of which are derived from first principles (see, e.g. [29–39]). However, it is difficult to identify generic relationships between potential parameters and macroscopic observables when using such complicated potentials. Furthermore, in many cases the potential parameters do not have immediate physical meaning for the bonding between atoms.

Here we use an alternative approach based on simple potentials describing the behaviour of model materials [40–44]. To investigate universal scaling behaviour between microscopic and macroscopic variables, this has been shown to be very fruitful and allows fundamental insight into the fracture mechanisms [32, 40–48].

By using simple model potentials, we deliberately avoid the complexities of sophisticated potential formulations. We adopt a simple pair potential based on a harmonic interatomic potential with spring constant k_0 in combination with a Lennard-Jones (LJ) potential to describe smooth bond breaking. The harmonic potential is chosen to model linear elastic material

Table 1. Elastic properties of the harmonic solid (analytical estimates according to equation (6)), and surface energy (evaluated numerically for the chosen simulation parameters described in section 2.2) across the LJ weak interface. The results agree reasonably well with the numerically calculated values of the elastic properties shown in figure 3.

Spring constant k_0	Young's modulus E	Poisson ratio ν	Surface energy γ (numerical result)
572	960	0.33	2.33

behaviour as assumed in Griffith's fracture theory. This allows us to define a clean and well-understood reference system.

Although simple pair potentials do not allow us to draw conclusions for unique phenomena pertaining to specific materials, they enable us to understand universal, generic relationships between potential shape and brittle fracture mechanics and adhesion properties of materials, and help elucidate the universal scaling laws of fracture mechanics.

To model a perfectly brittle solid, we assume harmonic interactions in the bulk of the strip,

$$\phi(r) = a_0 + \tfrac{1}{2}k_0(r - r_0)^2, \tag{4}$$

where k_0 is the spring constant, a_0 a reference constant and r_0 the nearest neighbour distance between immediate neighbours. Atoms in the bulk only interact with their nearest neighbours, and the bonds never break. Crack propagation is constrained along a weak fracture layer in the centre of the strip. To model bond breaking, we assume that atoms across this weak layer interact according to the 12–6 LJ potential

$$\phi(r) = 4\varepsilon\left(\left(\frac{\sigma}{r}\right)^{12} - \left(\frac{\sigma}{r}\right)^{6}\right). \tag{5}$$

We note that a similar setup has been used in [49]. In the simulations, we assume $\varepsilon = \sigma = 1$ and $r_0 = 2^{1/6} = 1.12246$ (FCC lattice constant $a = 1.587$). Interactions across the weak fracture layer (LJ potential) are cut off at a critical distance $r_{\text{cut}} = 2.5$. We modified the IMD code [28] so that the neighbouring tables are not updated during the simulation. Bonds only break between atoms that are located at different sides of the weak layer. This procedure ensures that the crack can only extend along a predefined direction.

For the analysis of the critical length for flaw tolerance, an exact knowledge of elastic properties and fracture surface energy is needed. It can be shown that Young's modulus is

$$E = \frac{4r_0^2}{3} \cdot k_0, \tag{6}$$

and the Poisson's ratio is given by $\nu = 1/3$. The elastic properties and fracture surface energy are summarized in table 1.

Figure 3 shows the elastic properties associated with a three-dimensional FCC crystal in the cubical orientation as used in our studies. The results obtained by numerical solution are in good accordance with the results obtained by using the analytical expressions (see table 1).

The surface energy is given by

$$\gamma = \tfrac{1}{2}N_{\text{b}}\rho_{\text{A}}\Delta\phi, \tag{7}$$

where N_{b} is the number of bonds per atom across the fracture path. The variable ρ_{A} corresponds to the density of surface atoms, and $\Delta\phi$ is the potential energy stored in each bond. For the (010) fracture surface, $\rho_{\text{A}} = 1/r_0^2 = 0.794$, and the parameter $N_{\text{b}} = 4$. The fracture surface energy for the simulation parameter used is given in table 1.

We emphasize that this setup of bulk material and a weak layer is particularly convenient for our studies because Young's modulus, E, can be easily varied independent of the other variables (γ and σ_{th}), allowing the critical length scale ξ_{cr} to be tuned in a range easily accessible to MD simulations.

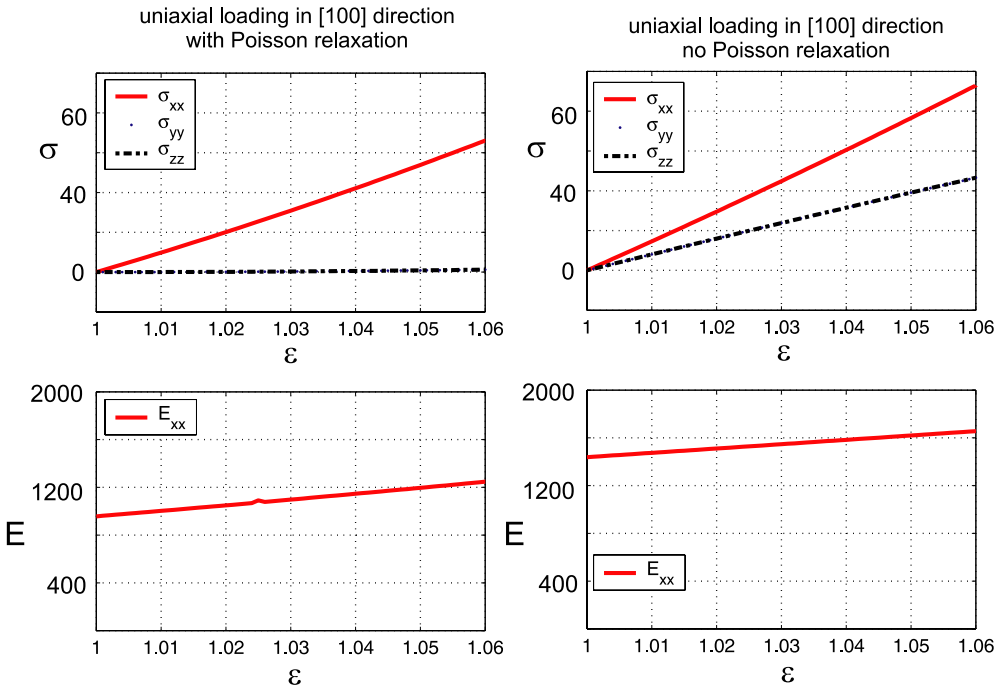

Figure 3. Elastic properties associated with the harmonic interatomic potential (see equation (4), $k_0 = 572$). The results for elastic properties obtained numerically are in good agreement with the values predicted by the analytical model. The left plots show the results obtained with Poisson relaxation (and consequently, σ_{zz} is zero), whereas the results on the right-hand side depict results obtained without Poisson relaxation. The plot shows that as expected, the harmonic potential leads to linear elastic material behaviour.

All simulation results are expressed in reduced units: energies are scaled by the depth of the LJ potential ε and lengths are scaled by σ. In these reduced units, the critical length scale is $\xi_{cr} = 119$ for the material parameters chosen in the simulation (this corresponds to a few tens of nanometres in real materials).

A critical element in our studies is the calculation of stresses from atomistic simulations. The atomic stress is calculated based on the virial theorem [50–52]. Recent investigations have shown that the atomistic definitions of stress near a moving crack tip show reasonable agreement with continuum mechanics predictions [40, 45, 53].

2.3. Simulation results: transition from Griffith governed failure by crack growth to uniform rupture at theoretical strength

Here we report simulation results on the size dependence of fracture strength of thin layers. In a series of studies, we calculate the critical fracture stress σ as a function of the material size (layer width ξ_{cr}).

Figure 4 shows the results of large-scale atomistic simulations of fracture strength of a small perfectly brittle platelet as a function of the inverse of the square root of the size of the material $\sqrt{\xi_{cr}/\xi}$. In the plot, we also include the predictions of Griffith's theory and the theoretical strength of the material.

Whereas the strength of the materials is well predicted by Griffith's theory for large dimensions ($\sqrt{\xi_{cr}/\xi} < 1$), reduction of dimension results in deviation from this prediction and

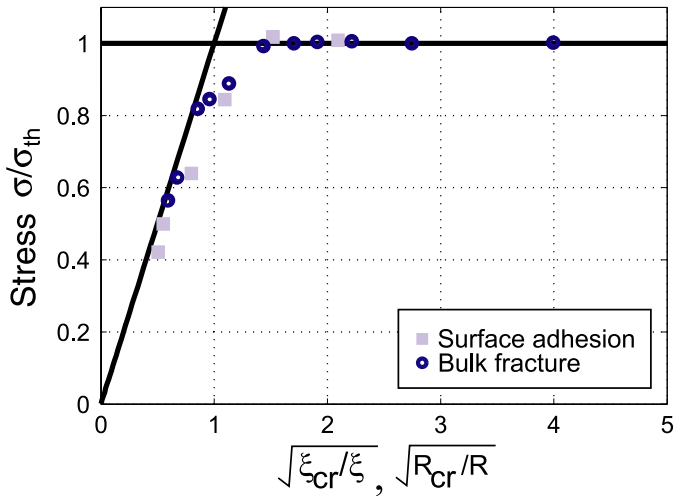

Figure 4. Fracture and adhesion strength as a function of the size of the material. The plot shows the results of bulk fracture as well as surface adhesion. The plot shows results normalized with respect to the theoretical strength and the critical length scale for flaw tolerance. These results suggest that the principle of dimension reduction is valid in a variety of systems, including surface adhesion (for a system as discussed in [16] consisting of an elastic punch on a rigid substrate) as well as bulk fracture [13].

eventually failure of the material at its theoretical strength σ_{th} regardless of the presence of flaws (for $\sqrt{\xi_{\text{cr}}/\xi} > 1$). This observation suggests a change in behaviour once the dimensions of the solid are below a critical length scale: the Griffith theory is no longer valid for extremely thin layer widths. We have made the calculation for different material parameters and the predictions by equation (3) are well reproduced in the simulations.

Now we focus on the stress distribution ahead of the crack slightly before failure occurs. In macroscopic systems and according to classical understanding, it is expected that the crack tip always constitutes a location of high stress concentration. Is this also true when the characteristic dimensions of the materials reach nanoscale?

Calculation of the stress distribution ahead of the crack reveals that the stress becomes increasingly homogeneous as the length scale of the structure decreases. In fact, we observe that the distribution becomes completely uniform for structural dimensions well below the critical length scale. This is in strong contrast to what we would expect based on a completely classical picture.

Further, we observe that the stress distribution does not change with structural size any more once the size of the material is below a critical value (this is observed for $\sqrt{\xi_{\text{cr}}/\xi} > 2.67$ in our simulations). The results are shown in figure 5. This size-independence of the fracture strength of materials is also in clear contrast to conventional knowledge. The results suggest that at nanoscale, materials may behave dramatically differently.

We note that behaviour similar to the one observed here for tensile loading is also expected for shear loading, as the underlying equations (1)–(3) take a similar form.

3. Adhesion strength of fibrillar structures

In this section, we focus on fibrillar adhesion structures as they appear in many biological systems, such as geckos.

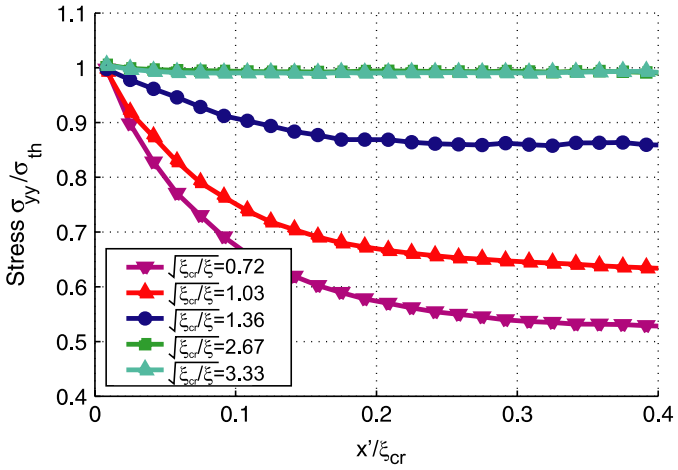

Figure 5. Stress distribution ahead of the crack in a thin mineral platelet just before failure, for different material sizes (the x-coordinate is scaled by the characteristic length scale x'/ξ_{cr}). The thinner the slab, the more homogeneous the stress distribution. When the slab width is smaller than the critical size, the stress distribution becomes homogeneous and does not depend on the size of the platelet any more (see values $\sqrt{\xi_{cr}/\xi} = 2.67$ and larger).

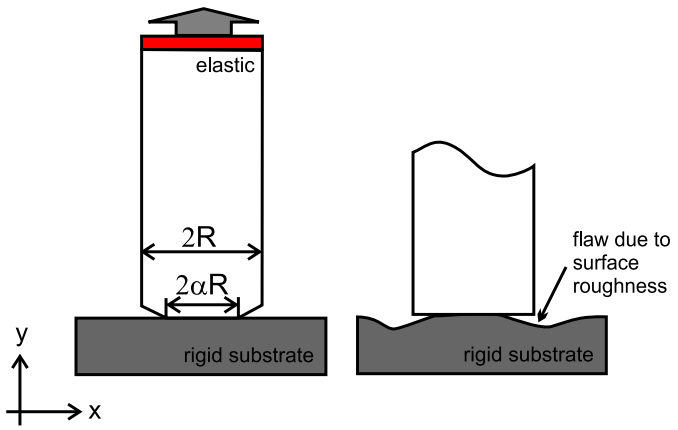

Figure 6. The schematic of the model used for studies of adhesion. The model represents a cylindrical Gecko spatula with radius R attached to a rigid substrate (left). A circumferential crack represents flaws for example resulting from surface roughness. The parameter α denotes the dimension of the crack. The area $0 < r < \alpha R$ corresponds to an area of perfect adhesion, whereas $\alpha R \leqslant r < R$ represents regions of no adhesion. This model resembles the effect of surface roughness as depicted schematically on the right-hand side.

3.1. Theoretical considerations of size reduction of adhesion elements

To understand adhesion properties at small scales, we have modelled an elastic flat-ended cylindrical hair in adhesive contact with a rigid substrate [16]. The radius of the cylinder is R. To test the ability of the flat cylinder to adhere in the presence of adhesive flaws, imperfect contact between the spatula and substrate is assumed such that the radius of the actual contact area is $a = \alpha \cdot R$, where $0 < \alpha < 1$, as shown in figure 6 (left); the outer rim $\alpha \cdot R < r < R$ represents flaws or regions of poor adhesion. In our present model, which is similar to a

continuum model in [54], there is no adhesion in the region $\alpha \cdot R < r < R$, and so the model resembles a cylinder attached to the substrate with a circumferential crack.

The adhesive strength of such an adhesive joint can be calculated by treating the contact problem as a circumferentially cracked cylinder, in which case the stress field near the edge of the contact area has a square-root singularity with stress intensity factor

$$K_I = \frac{P}{\pi a^2}\sqrt{\pi a}F_1(\alpha), \tag{8}$$

where $F_1(\alpha)$ varies in a narrow range between 0.4 and 0.5 for $0 < \alpha < 0.8$ ($\alpha = 1$ corresponds to perfect, defect-free contact). We substitute equation (8) into the Griffith condition

$$\frac{K_I^2}{2E^*} = \Delta\gamma, \tag{9}$$

where the numerical factor of 2 is due to the rigid substrate. The apparent adhesive strength normalized by the theoretical strength for adhesion, $\hat{\sigma}_c = P_c/(\pi\sigma_{th}R^2)$, is obtained as

$$\hat{\sigma}_c = \beta\alpha^2\psi, \tag{10}$$

where

$$\psi = \sqrt{\frac{\Delta\gamma E^*}{R\sigma_{th}^2}} \tag{11}$$

and

$$\beta = \sqrt{2/(\pi\alpha F_1^2(\alpha))} \qquad \text{as well as } E^* = E/(1-\nu^2), \tag{12}$$

while E and ν are the Young's modulus and Poisson ratio, respectively.

The adhesive strength is a linear function of the dimensionless variable Ψ with slope $\beta\alpha^2$. The maximum adhesion strength is achieved when the pull-off force reaches $P_c = \sigma_{th}\pi a^2$, or $\hat{\sigma}_c = \alpha^2$, in which case the traction within the contact area uniformly reaches the theoretical strength σ_{th}. This saturation in strength occurs at a critical size of the contact area

$$R_{cr} = \beta^2\frac{\Delta\gamma E^*}{\sigma_{th}^2} \tag{13}$$

This length scale corresponds to ξ_{cr} described in section 2.1 (equation (3)).

3.2. Theoretical considerations of shape optimization of adhesion elements

The results in the previous sections indicate that optimal adhesion and optimal fracture strength can be achieved by reducing the dimension of the structure.

In this section, we focus on the question: can optimal adhesion be achieved at any size of the punch? The system of interest is a periodic array of rigid punches attached to an elastic substrate as schematically shown in figure 7 in a quasi-two-dimensional geometry with periodic boundary conditions.

The reader is referred to [19] for discussions on the concepts of optimal and singular shapes in adhesive contact mechanics. For a single punch, it can be shown that the optimal shape is given by

$$z = -\psi\frac{2\sigma_{th}R}{\pi E/(1-\nu^2)}\left[\ln\left(1-\bar{r}^2\right) + \bar{r}\ln\left(\frac{1+\bar{r}}{1-\bar{r}}\right)\right] \tag{14}$$

for $\psi = 1$. Here $0 \leqslant \psi \leqslant 1$ is used as a shape parameter to vary the shape from singular $\psi = 0$ to optimal $\psi = 1$. Note that $\bar{r} = r/R$ denotes a reduced radius (so that $0 \leqslant \bar{z} \leqslant 1$).

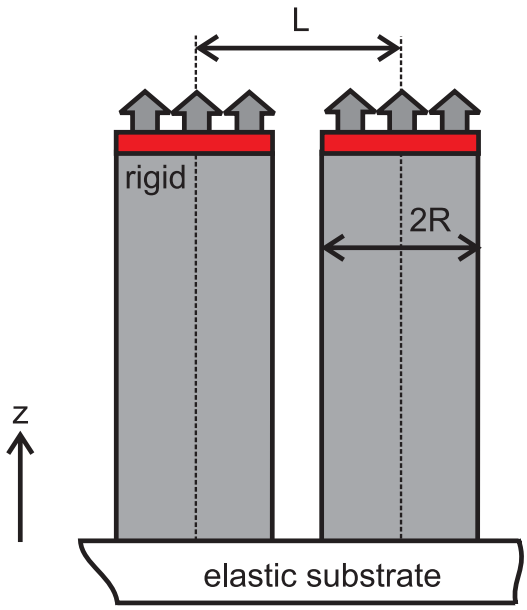

Figure 7. The geometry of the system considered is a periodic array of punches of radius R. The rigid–elastic interface leads to singular stress concentrations for flat punches. We vary the shape of the rigid punch surfaces to avoid these singular stress concentrations.

For a punch array, the optimal shape is given by a series expression

$$z = -\psi \frac{2\sigma_{\mathrm{th}} R}{\pi E/(1-\nu^2)} \left\{ \left[\ln\left(1-\bar{r}^2\right) + \bar{r} \ln\left(\frac{1+\bar{r}}{1-\bar{r}}\right) \right] - \sum_{n=1}^{\infty} \left[\ln\left(\frac{(2n\lambda+\bar{r})^2-1}{(2n\lambda)^2-1}\right) + (2n\lambda+\bar{r}) \ln\left(\frac{2n\lambda+\bar{r}+1}{2n\lambda+\bar{r}-1}\right) - 2n\lambda \ln\left(\frac{2n\lambda+1}{2n\lambda-1}\right) \right] - \sum_{n=1}^{\infty} \left[\ln\left(\frac{(2n\lambda-\bar{r})^2-1}{(2n\lambda)^2-1}\right) + (2n\lambda-\bar{r}) \ln\left(\frac{2n\lambda-\bar{r}+1}{2n\lambda-\bar{r}-1}\right) - 2n\lambda \ln\left(\frac{2n\lambda+1}{2n\lambda-1}\right) \right] \right\}. \tag{15}$$

where $\lambda = L/R$ denotes the ratio of the total length of each unit cell to the radius (in the numerical examples we consider a periodic array of spatulas with $\lambda = 1.33$). The theoretical prediction of the optimal shape as a function of the shape parameter ψ is shown in figure 8.

The critical length scale for a single fibre on a substrate (in analogy to equations (3) and (13)) is given by

$$R_{\mathrm{cr}} = \frac{8}{\pi} \frac{E^* \Delta\gamma}{\sigma_{\mathrm{th}}^2}. \tag{16}$$

3.3. Atomistic modelling

The simulation geometry of the atomistic studies discussed in this section is shown in figure 6 (studies of size reduction only) and figure 7 (studies of shape variation). In the first case, the punch is elastic and the substrate is rigid (figure 6), and in the second case, the punch is rigid

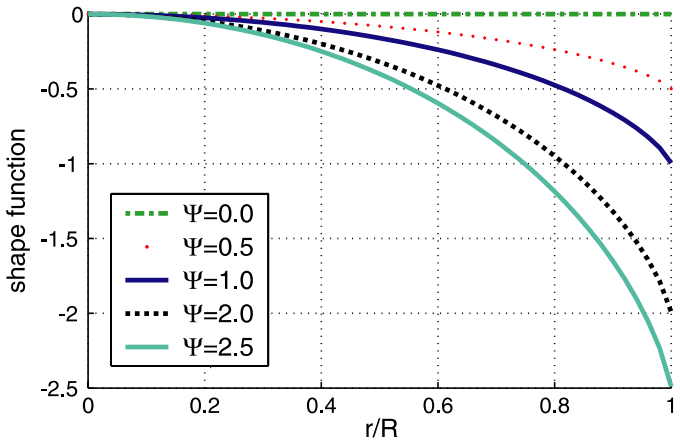

Figure 8. The shape function defining the surface shape change as a function of the shape parameter. For $\psi = 1$, the optimal shape is reached and stress concentrations are predicted to disappear.

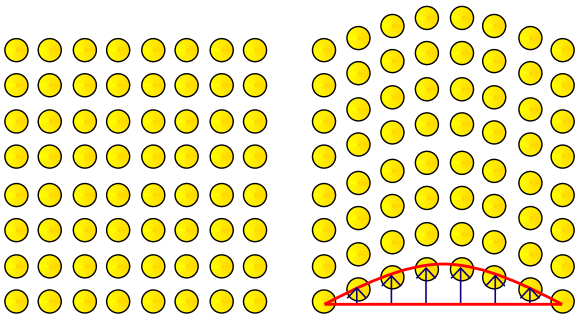

Figure 9. Atom rows in the rigid punch are displaced according to the continuum mechanics solution of the optimal surface shape (for theoretical solution see figure 8 or equation (15)). This method allows achieving a smoothly varying surface and enables a continuous transition from a flat punch (left) to the optimal shape (right).

and the substrate is elastic (figure 7). This is in accordance with the continuum mechanics models described in sections 3.1 and 3.2.

In both cases, we model the elastic part using a harmonic potential (here with $k_0 = 57.2$, see equation (4)), and we treat the interface between the two parts using a Lennard-Jones potential (see equation (5)) to model the vdW interactions. The expressions for the interatomic potentials, as well as the overall simulation method, including the expressions for elastic properties and fracture surface energy are identical to the procedure described in section 2.2 and therefore are not repeated here. We note that this Griffith type approach to adhesion has been well established by the JKR model in adhesive contact mechanics [55].

Studies on the variations of surface shape require a method for achieving small and smooth variations of surface shape in atomistic models. Such a change in surface shape is achieved by displacing the rows of atoms as shown in figure 9. This method allows achieving a smoothly varying surface in the MD simulations. We note that the alternative approach in cutting the optimal shape out of an atomic lattice does not work well because of the discreteness of the lattice and the resulting steps on the order of Burgers vector.

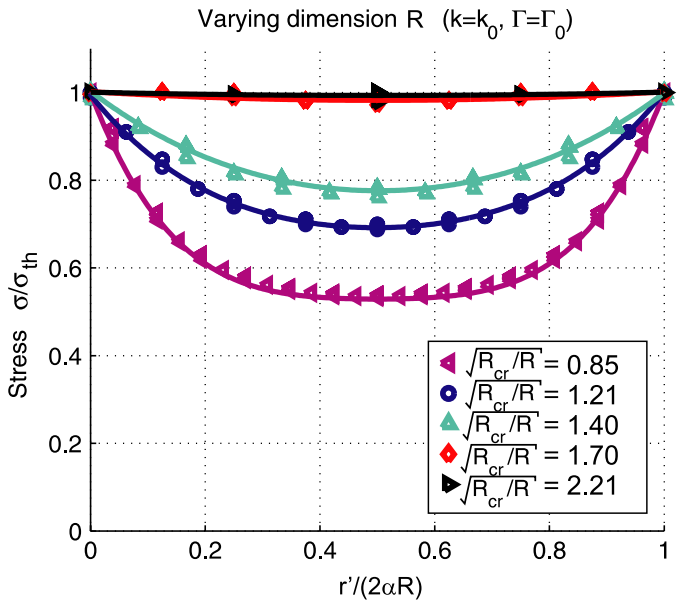

Figure 10. Stress distribution in the elastic punch slightly before complete detachment (the stress is calculated in a thin strip along the diameter, within the area of contact $R_{\text{cut}} = 2\alpha R$). The simulations reveal that for large radii, a stress concentration develops at the exterior sides of the cylinder. For small dimensions, this stress distribution starts to vanish. For dimensions smaller than the critical radius for flaw tolerance (large ratios of $\sqrt{R_{\text{cr}}/R}$), the stress distribution becomes homogeneous and does not vary with the cylinder diameter any more.

3.4. Simulation results

Here we report the results of a series of computational experiments with the models described in the previous section.

The first question we address is how the adhesion strength varies with the diameter of the spatula. Figure 4 shows the results of large-scale atomistic simulations of adhesion strength as a function of the size of the material R/R_{cr} (corresponding to the geometry shown in figure 6). Whereas the strength of the materials interfaces is predicted reasonably well based on Griffith's theory for large dimensions, reduction of dimension results in deviation from this prediction and eventually failure of the material at its theoretical strength σ_{th} regardless of the presence of the flaw. In practical terms, that means even if there is surface roughness present, the roughness does *not* lead to stress concentrations and the adhesion device adheres robustly to the substrate.

We now focus on the stress distribution across the adhesion element slightly before detachment occurs. We vary (i) the dimensions of the adhesion element, (ii) the adhesion energy and (iii) the elastic properties of the substrate. We consider a rigid punch on an elastic substrate.

Figure 10 shows the stress distribution at the punch-substrate interface close to detachment for various choices of the ratio R/R_{cr}. The simulations reveal that for large radii, a stress concentration develops at the exterior sides of the cylinder. This result is expected from the classical understanding of fracture mechanics and corresponds to the regime where Griffith's theory holds to describe the onset of detachment. For small dimensions, the stress distribution starts to become uniform. For dimensions smaller than the critical radius for flaw tolerance, the stress distribution becomes homogeneous and does not vary with the diameter of the cylinder any more.

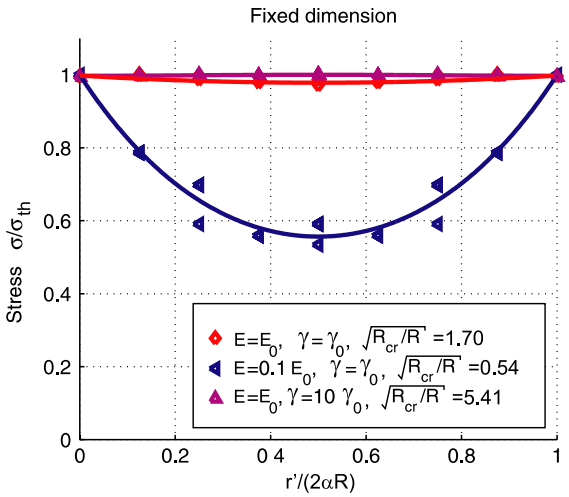

Figure 11. Stress distribution in the elastic punch slightly before complete detachment (the stress is calculated in a thin strip along the diameter, within the area of contact $R_{\text{cut}} = 2\alpha R$). Here we keep the dimension fixed and vary the adhesion energy (γ_0 corresponds to the surface energy shown in table 1) and the elastic properties (E_0 corresponds to Young's modulus obtained for $k_0 = 57.23$). We find that the stress distribution becomes homogeneous for large ratios of $\sqrt{R_{\text{cr}}/R}$, in agreement with the other results (see figures 5 and 11).

Figure 11 shows variations of the stress distribution close to detachment for changes in adhesion energy and elastic properties of the substrate. These results further support the notion that

$$R_{\text{cr}} \sim E \tag{17}$$

and

$$R_{\text{cr}} \sim \gamma \tag{18}$$

as suggested by equations (3), (13) and (16).

We now focus on change in the adhesion strength due to variations in the surface shape. Our atomistic studies are based on the continuum considerations reported in section 3.2 where we discussed a surface shape that would always lead to optimal adhesion, at any length scale. Figure 12 shows the stress distribution along the diameter of the punch for different choices of the shape parameter describing the punch shape. The results indicate that when the optimal shape is reached ($\psi = 1$), the stress distribution is completely flat as in the homogeneous case ($\lambda = 1$) without stress magnification. We observe that for $\psi < 1$, a stress concentration develops at the boundaries of the punch, whereas for $\psi > 1$ the largest stress occurs in the centre.

Figure 13 shows the maximum adhesion strength as a function of the shape parameter ψ for different sizes of the punch. These observations allow drawing conclusions about the robustness: Our results indicate that although optimal adhesion can be achieved at any length scale by changing the shape of the attachment device (by choosing $\psi = 1$), robustness with respect to variations in shape while at the same time keeping a strong adhesion force can only be achieved at small length scales.

Robustness thus seems to be closely coupled to nano-dimensioned adhesion systems. We believe that only reduction in length scale results in (1) robustness and (2) disappearance of the stress concentration. This may explain why nature does not primarily optimize shape but instead focuses on reduction of dimension as a design strategy [13, 17, 20].

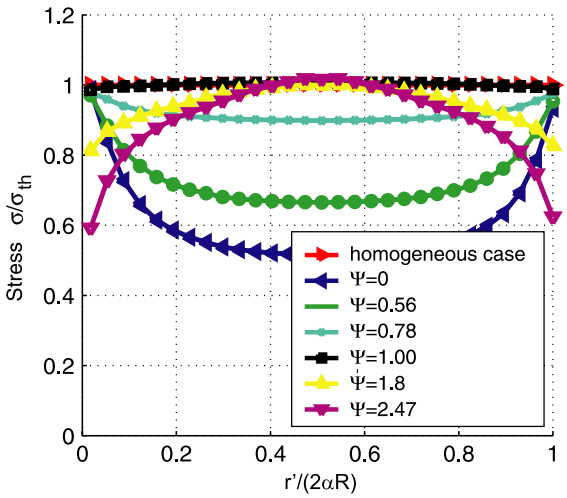

Figure 12. Stress distribution along the diameter of the punch for different choices of the shape parameter describing the punch shape. The results indicate that when the optimal shape is reached ($\psi = 1$), the stress distribution is completely flat as in the homogeneous case ($\lambda = 1$) without stress magnification. We observe that for $\psi < 1$, a stress concentration develops at the boundaries of the punch, whereas for $\psi < 1$ the largest stress occurs in the centre.

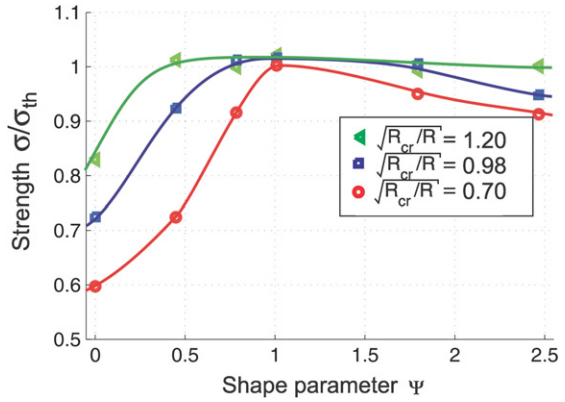

Figure 13. Adhesion strength for different choices of the shape parameter ψ. The results indicate that although optimal adhesion can be achieved at any length scale by changing the shape of the attachment device (by choosing $\psi = 1$), robustness with respect to variations in shape while at the same time keeping a strong adhesion force can only be achieved at small length scales.

4. Discussion and conclusions

We have used continuum and atomistic concepts to investigate how the fracture and failure behaviours of materials change as a function of size. The atomistic simulations reveal a smooth transition between the Griffith mode of failure via crack propagation to uniform bond rupture at theoretical strength below a nanometre critical length, as shown in figure 5 for both fracture of a nanoparticle and surface adhesion of an elastic punch on a rigid substrate (see figures 10 and 11). We find that below a critical length ξ_{cr} (or R_{cr}, for adhesion systems), the stress distribution

becomes uniform near the crack tip. The atomistic simulations fully support the hypothesis that materials become insensitive to flaws below a critical nanometre length scale ξ_{cr}.

Our results corroborate earlier suggestions made at the continuum level [13, 16] that the concept of nanoscale flaw tolerance may play a critical role in developing structural links in biological materials, as many biological materials feature small nanoscale dimensions. This may suggest common design principles in order to improve some mechanical properties of materials:

> *Small nano-substructures lead to robust, flaw-tolerant materials. Nature may have used this principle to build strong structural materials.*

Surprisingly, this principle is found in different geometries and cases, including bulk and surface materials. Our results extend the notion 'smaller is stronger' to 'nano is optimal'. Our studies on adhesion systems indicate that optimal adhesion can be achieved at any scale if the adhesion surface shape is adapted to eliminate locations of stress concentration (see figure 12). However, this design strategy does not lead to robust adhesion elements as the smallest deviations from the optimal shape lead to catastrophic failure (see figure 13). We find that reduction in the diameter of cylindrical adhesion systems leads to optimal adhesion including robustness; therefore, 'nano is also robust'. We note that the actual displacements of atoms necessary to realize the optimal shape are on the order of a few angstroms. Due to the discrete nature of atoms with typical distances between 1–3 Å, realization of the optimal shape at such small scales may become difficult. This may be another, alternative reason why shape optimization is not a preferred strategy to achieve optimal adhesion. We refer the reader to other articles for a more detailed discussion of linking the flaw-tolerance concept to biological materials [13, 16, 54].

Atomistic modelling has proved to be a powerful tool in designing virtual experiments to demonstrate the concept and effect of size reduction and shape changes. Unlike purely continuum mechanics theories, MD simulations can intrinsically handle stress concentrations (singularities) well and provide accurate descriptions of bond breaking. Also, it can be straightforwardly used to study ultra-small scale systems, thus probing the limiting cases where continuum theories start to break down. Our approach of using simplistic model potentials rather than utilizing highly complex expressions for the atomic interactions allows us to carry out fundamental parameter studies enabling immediate comparison with continuum theories. Even though our results do not allow us to make quantitative predictions about specific materials, our studies may help to develop a deeper understanding of the mechanics of brittle fracture at nanoscale. However, recent progress in developing atomistic and molecular models of biological materials such as collagen [22] provide a fundamental, quantitative viewpoint of the mechanics of such chemically complex biological materials, with structural details spanning several length scales.

The increase in computing power allows, at the same time, modelling at length scales on the order of micrometers. We believe that atomistic-based modelling could play a significant role in the future in the area of modelling nano-mechanical phenomena and linking them to continuum mechanical theories as exemplified in this article.

Acknowledgments

MJB acknowledges the assitance given by the Institute for Theoretical and Applied Physics at the University of Stuttgart through provision of their MD simulation code [28]. He also acknowledges support from the CEE Department at MIT. Support of this work has also been provided by the National Science Foundation of China and the Chang Jiang Scholarship

programme of the through Tsinghua University. Most of the large-scale atomistic calculations were carried out at the MARS LINUX cluster at the Max Planck Institute for Metals Research in Stuttgart.

References

[1] Farkas D, Swygenhoven H v and Derlet P 2002 Intergranular fracture in nanocrystalline metals *Phys. Rev.* B **66** 184112
[2] Swygenhoven H v *et al* 1999 Competing plastic deformation mechanisms in nanophase metals *Phys. Rev.* B **60** 22–5
[3] Yamakov V *et al* 2003 Deformation mechanism crossover and mechanical behaviour in nanocrystalline materials *Phil. Mag. Lett.* **83** 385–93
[4] Wolf D *et al* 2003 Deformation mechanism and inverse Hall–Petch behavior in nanocrystalline materials *Z. Metallk* **94** 1052–61
[5] Yamakov V *et al* 2002 Grain-boundary diffusion creep in nanocrystalline palladium by molecular-dynamics simulation *Acta Mater.* **50** 61–73
[6] Van Swygenhoven H, Derlet P M and Froseth A G 2004 Stacking fault energies and slip in nanocrystalline metals *Nature Mater.* **3** 399–403
[7] Yamakov V *et al* 2004 Deformation-mechanism map for nanocrystalline metals by molecular-dynamics simulation *Nature Mater.* **3** 43–7
[8] Buehler M J, Hartmaier A and Gao H 2004 Hierarchical multi-scale modeling of plasticity of submicron thin metal films *Modelling Simul. Mater. Sci. Eng.* **12** S391–413
[9] Buehler M J, Hartmaier A and Gao H 2003 Atomistic and continuum studies of crack-like diffusion wedges and dislocations in submicron thin films *J. Mech. Phys. Solids* **51** 2105–25
[10] Hartmaier A, Buehler M J and Gao H J 2005 Two-dimensional discrete dislocation models of deformation in polycrystalline thin metal films on substrates *Mater. Sci. Eng. A—Struct. Mater. Prop. Microstruc. Process.* **400** 260–3
[11] Hartmaier A, Buehler M J and Gao H J 2005 Multiscale modeling of deformation in polycrystalline thin metal films on substrates *Adv. Eng. Mater.* **7** 165–9
[12] Arzt E 1998 Size effects in materials due to microstructural and dimensional constraints: a comparative review *Acta Mater.* **46** 5611–26
[13] Gao H *et al* 2003 Materials become insensitive to flaws at nanoscale: lessons from nature *Proc. Natl Acad. Sci. USA* **100** 5597–600
[14] Gao H *et al* 2004 Flaw tolerant bulk and surface nanostructures of biological systems *Mech. Chem. Biosys.* **1** 37–52
[15] Gao H and Ji B 2003 Modeling fracture in Nano-materials via a Virtual Internal Bound Method *Eng. Fract. Mech.* **70** 1777–91
[16] Gao H and Yao H 2004 Shape insensitive optimal adhesion of nanoscale fibrillar structures *Proc. Natl Acad. Sci. USA* **101** 7851–6
[17] Arzt E, Gorb S and Spolenak R 2003 From micro to nano contacts in biological attachment devices *Proc. Natl Acad. Sci. USA* **100** 10603–6
[18] Okumara K and Gennes P-G d 2001 Why is nacre strong? Elastic theory and fracture mechanics for biocomposites with stratified structures *Eur. Phys. J.* E **4** 121–7
[19] Scherge M and Gorb S N 2001 *Biological Micro and Nano-tribology* (New York: Springer)
[20] Arzt E, Enders S and Gorb S 2002 Towards a micromechanical understanding of biological surface devices *Z. Metallk.* **93** 345–51
[21] Persson B N J 2003 On the mechanism of adhesion in biological systems *J. Chem. Phys.* **118** 7614–21
[22] Buehler M J 2006 Atomistic and continuum modeling of mechanical properties of collagen: elasticity, fracture and self-assembly *J. Mater. Res.* at press
[23] Jager I and Fratzl P 2000 Mineralized collagen fibrils: a mechanical model with a staggered arrangement of mineral particles *Biophys. J.* **79** 1737–46
[24] Autumn K *et al* 2002 Evidence for van der Waals adhesion in gecko setae *Proc. Natl Acad. Sci. USA* **99** 12252–6
[25] Griffith A A 1920 The phenomenon of rupture and flows in solids *Phil. Trans. R. Soc.* A **221** 163–98
[26] Anderson T L 1991 *Fracture Mechanics: Fundamentals and Applications* (Boca Raton, FL: CRC Press)
[27] Gao H J and S H Chen 2005 Flaw tolerance in a thin strip under tension *J. Appl. Mech.—Trans. ASME* **72** 732–7
[28] Stadler J, Mikulla R and Trebin H-R 1997 IMD: a software package for molecular dynamics studies on parallel computers *Int. J. Mod. Phys.* C **8** 1131–40

[29] Abraham F F and Gao H 1998 Anamalous brittle-ductile fracture behaviors in FCC crystalsy *Phil. Mag. Lett.* **78** 307–12
[30] Baskes M I 1997 Determination of modified embedded atom method parameters for nickel *Mater. Chem. Phys.* **50** 152–8
[31] Duin A C T v *et al* 2001 ReaxFF: a reactive force field for hydrocarbons *J. Phys. Chem.* A **105** 9396–409
[32] Buehler M J, Duin A C T v and Goddard W A 2006 Multi-paradigm modeling of dynamical crack propagation in silicon using the ReaxFF reactive force field *Phys. Rev. Lett.* **96** 095505
[33] Thijsse B J 2005 Silicon potentials under (ion) attack: towards a new MEAM model *Nucl. Instrum. Methods Phys. Res.* **228** 198–211.
[34] Tersoff J 1988 Empirical interatomic potentials for carbon, with applications to amorphous carbon *Phys. Rev. Lett.* **61** 2879–83
[35] Mishin Y *et al* 2001 Structural stability and lattice defects in copper: *ab-initio*, tight-binding and embedded-atom calculations *Phys. Rev.* B **63** 224106
[36] Abraham F F *et al* 2000 Dynamic fracture of silicon: concurrent simulation of quantum electrons, classical atoms, and the continuum solid *MRS Bull.* **25** 27–32
[37] Duin A C T v *et al* 2003 ReaxFF SiO: reactive force field for silicon and silicon oxide systems *J. Phys. Chem.* A **107** 3803–11
[38] Holland D and Marder M 1998 Ideal brittle fracture of silicon studied with molecular dynamics *Phys. Rev. Lett.* **80** 746
[39] Swadener J G, Baskes M I and Nastasi M 2002 Molecular dynamics simulation of brittle fracture in silicon *Phys. Rev. Lett.* **89** 085503
[40] Buehler M J and Gao H 2006 Dynamical fracture instabilities due to local hyperelasticity at crack tips *Nature* **439** 307–10
[41] Buehler M J, Abraham F F and Gao H 2003 Hyperelasticity governs dynamic fracture at a critical length scale *Nature* **426** 141–6
[42] Abraham F F *et al* 1997 A molecular dynamics investigation of rapid fracture mechanics *J. Mech. Phys. Solids* **45** 1595–19
[43] Abraham F F 1996 Dynamics of brittle fracture with variable elasticity *Phys. Rev. Lett.* **77** 869
[44] Abraham F F *et al* 1994 Instability dynamics of fracture: a computer simulation investigation *Phys. Rev. Lett.* **73** 272–5
[45] Buehler M J, Abraham F F and Gao H 2004 Stress and energy flow field near a rapidly propagating mode I crack *Springer Lecture Notes Computational Science Engigeneering* ISBN 3-540-21180-2, pp 143–56
[46] Abraham F F and Gao H 2000 How fast can cracks propagate? *Phys. Rev. Lett.* **84** 3113–16
[47] Abraham F F *et al* 2002 Simulating materials failure by using up to one billion atoms and the world's fastest computer: work-hardening *Proc. Natl Acad. Sci. USA* **99** 5783–7
[48] Abraham F F *et al* 2002 Simulating materials failure by using up to one billion atoms and the world's fastest computer: brittle fracture *Proc. Natl Acad. Sci. USA* **99** 5788–92
[49] Movchan A B, Bullough R and Willis J R 2003 Two-dimensional lattice models of the Peierls type *Phil. Mag.* **83** 569–87
[50] Zhou M and McDowell D L 2002 Equivalent continuum for dynamically deforming atomistic particle systems *Phil. Mag.* A **82** 2547–74
[51] Tsai D H 1979 Virial theorem and stress calculation in molecular-dynamics *J. Chem. Phys.* **70** 1375–82
[52] Zimmerman J A *et al* 2004 Calculation of stress in atomistic simulation *Modelling. Simul. Mater. Sci. Eng.* **12** S319–32
[53] Buehler M J, Gao H and Huang Y 2003 Continuum and atomistic studies of a suddenly stopping supersonic crack computational *Mater. Sci.* **28** 385–408
[54] Gao H *et al* 2005 Mechanics of hierarchical adhesion structures of geckos *Mech. Mater.* **37** 275–85
[55] Johnson K L 1971 Surface energy and contact of elastic solids *Proc. R. Soc.* A **324** 301